



HAL
open science

High resolution X-ray tomography of micromechanisms of fatigue crack closure

Kern Hauw Khor, Jean-Yves Buffiere, Wolfgang Ludwig, Ian Sinclair

► **To cite this version:**

Kern Hauw Khor, Jean-Yves Buffiere, Wolfgang Ludwig, Ian Sinclair. High resolution X-ray tomography of micromechanisms of fatigue crack closure. *Scripta Materialia*, 2006, 55 (1), pp.47-50. 10.1016/j.scriptamat.2006.01.016 . hal-00436213

HAL Id: hal-00436213

<https://hal.science/hal-00436213>

Submitted on 23 Apr 2024

HAL is a multi-disciplinary open access archive for the deposit and dissemination of scientific research documents, whether they are published or not. The documents may come from teaching and research institutions in France or abroad, or from public or private research centers.

L'archive ouverte pluridisciplinaire **HAL**, est destinée au dépôt et à la diffusion de documents scientifiques de niveau recherche, publiés ou non, émanant des établissements d'enseignement et de recherche français ou étrangers, des laboratoires publics ou privés.

High resolution X-ray tomography of micromechanisms of fatigue crack closure

K.H. Khor,^a J.-Y. Buffière,^b W. Ludwig^c and I. Sinclair^{a,*}

^aMaterials Research Group, School of Engineering Sciences, University of Southampton, Southampton SO17 1BJ, United Kingdom

^bGEMPPM UMR CNRS 5510, INSA, Lyon, France

^cCNRS/European Synchrotron Radiation Facility, 6 rue J. Horowitz, 38042 Grenoble, France

Abstract—Fatigue crack closure has been studied in an aluminium alloy via microtomography. Gallium wetting has been used to visualise grain structure, along with electron backscattered diffraction assessment of grain orientations and crack trajectories. Through this synthesis of techniques, a detailed direct assessment of microstructure and closure micromechanisms has been achieved.

Keywords: Microtomography; Fatigue; Closure; Crystallography; Slip band failure

1. Introduction

Fatigue crack closure has been recognised to play a significant role in microstructural contributions to fatigue crack growth resistance in various metallic materials [1–4]. This is frequently related to roughness induced crack closure (RICC), where local crack path perturbations from a nominal maximum tensile opening plane lead to asperity contacts in the crack wake [2–6]. Such crack path perturbations have been linked to factors such as crystallographic crack growth and the presence of duplex/multiphase microstructures [5,6].

Stress states are known to play a fundamental role in crack closure, particularly in the efficacy of plasticity induced crack closure [4]. With conventional microscopic *in situ* observations of crack behaviour in metallic systems being constrained to near-surface, plane stress dominated behaviour, the availability of sub-micron resolution X-ray tomography provides a valuable opportunity to resolve internal, mechanically constrained crack behaviour [7–10]. Given the dependency of crack closure processes on local microstructural influence, the present work seeks to synthesise such observations with detailed two- and three-dimensional microstructural characterisation.

2. Materials and experimental methods

Given the importance of establishing steady state crack growth conditions in assessing long crack closure [4], conventional three-point bend fatigue tests were carried out in general accord with British/ISO Standard 12108:2002 [11] on a commercial 2024-type airframe aluminium plate (in the naturally aged, T351 condition), see Figure 1. Fatigue testing of the bend specimens was carried out at a load ratio (R) of 0.1 and a frequency of 20 Hz, in an L – T orientation relative to the plate working direction. Load shedding was employed down to a near-threshold condition, identified here with a nominal ΔK of 6 MPa $\sqrt{\text{m}}$. Growth was then sustained over a distance in excess of 0.5 mm, corresponding to some 10 plane strain maximum plastic zone dimensions (given a material yield strength of ~ 390 MPa in the loading direction). Electron backscattered diffraction (EBSD) observations showed the material to be predominantly un-recrystallised (recrystallised fraction of $\sim 8\%$), presenting a highly elongated, pancake grain structure, with a mean free path between high angle boundaries of 40 μm in the short transverse direction.

In situ high resolution microtomographic imaging required a sample cross-section of $\sim 1 \times 1$ mm, see Figure 1(b) and (c). As such, ‘matchstick’ samples were prepared from the larger bend samples: the bend sample was sectioned using a low speed diamond saw to minimise

* Corresponding author; e-mail: is1@soton.ac.uk

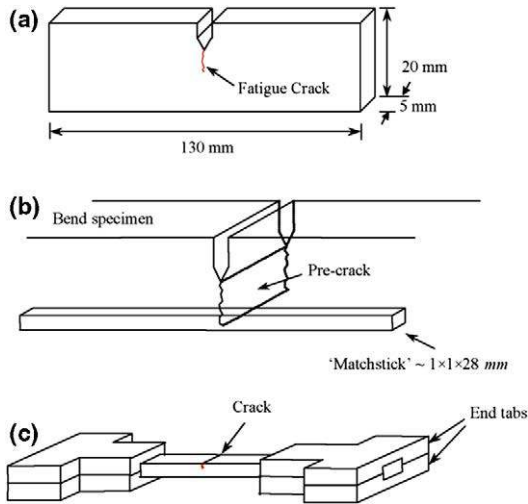


Figure 1. Schematic representation of (a) the geometry of the bend test fatigue sample, (b) extraction of matchstick sample from the original band specimen, and (c) bonding of end tabs to the matchstick sample.

mechanical disturbance of the underlying material, and, via a carefully gauged series of cuts, matchsticks containing the original fatigue crack tip were prepared with the crack at the approximate mid-thickness of the matchstick (i.e. a crack length of $\sim 500 \mu\text{m}$ was retained). Brass tabs were then glued to the sample ends for subsequent loading. Great care was exerted to prevent any mechanical damage or distortion of the cracked matchstick coupons, with alignment of the loading tabs being achieved by the use of an adjustable supporting jig.

Microtomographic observations were performed to an isotropic voxel size of $0.7 \mu\text{m}$ at beamline ID19 of the European Synchrotron Radiation Facility (ESRF). A beam energy of 20 keV was utilised, with a sample to detector distance of 50 mm providing enhanced edge detection via near-field Fresnel diffraction (phase con-

trast) [12]. Radiographs (1500) were recorded for a 180° rotation, with flat field and dark current corrections being obtained prior to reconstruction via filtered back-projection. Image analysis, segmentation and 3D rendering were carried out using a commercial software package (Volume Graphics GmbH, VGStudio Max). *In situ* imaging of cracks was carried out on the matchstick samples using a specially designed loading frame; crack lengths in individual samples were measured and suitable static uniaxial loads calculated and applied to achieve stress intensity levels up to the maximum applied during the final stage of crack growth in the original bend coupon (i.e. $6.67 \text{ MPa}\sqrt{\text{m}}$ for a ΔK of $6 \text{ MPa}\sqrt{\text{m}}$ and R of 0.1).

Following the *in situ* crack loading observations, samples were subjected to a liquid gallium (Ga) grain boundary wetting to highlight the grain boundaries [12] under subsequent tomographic imaging. This was followed by post mortem metallographic sectioning and EBSD analysis of the samples.

3. Results and discussion

Figure 2 shows typical tomographic sections of a fatigue cracked sample, before and after liquid Ga treatment, whilst Figure 3(a) shows segmented three dimensional (3D) representations of the same region where the crack volume extracted (running across the image) and the grain boundaries (running from top-to-bottom in the image) are superimposed in Figure 3(b). Correlation with EBSD data showed the majority of high angle boundaries to be identified by Ga charging, although a number were faint or absent, e.g. locations marked Z1–Z4 in Figure 2(b). In the first instance, such absences may be identified with special boundary orientations, as Ga take-up is driven by effective interface energies, see Refs. [12,13]. It may be noted that whilst

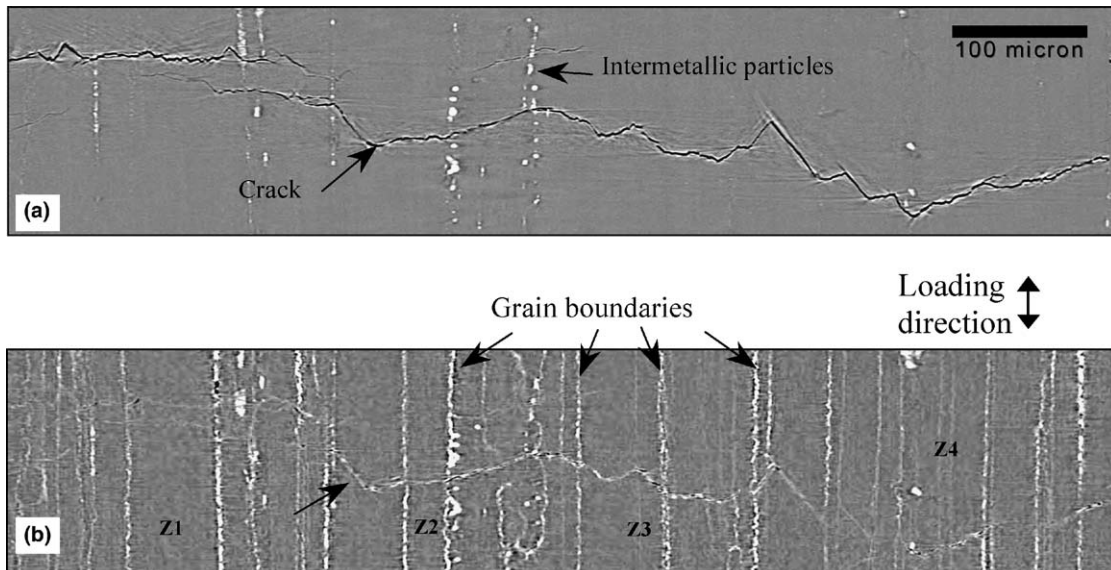


Figure 2. 2D slices of tomographic dataset showing cross-sectional view (L - S plane) of a crack mouth: (a) before and (b) after application of liquid Ga. Crack growth direction is normal the image plane.

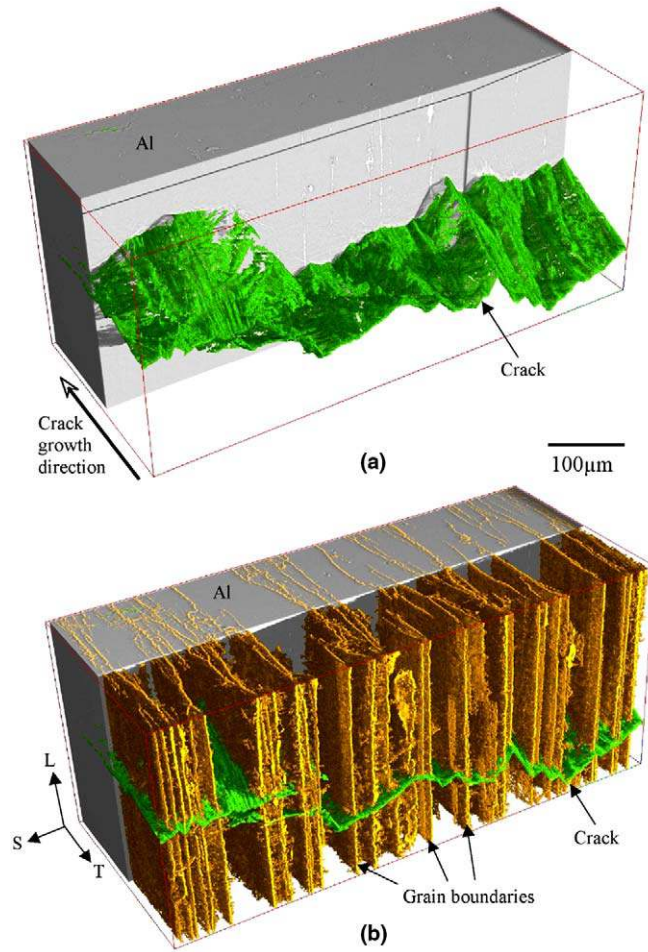


Figure 3. 3D representations of the crack region associated with the sections in Figure 2, highlighting: (a) the crack volume (green), and (b) grain boundaries (yellow). (For interpretation of the references in color in this figure legend, the reader is referred to the web version of this article.)

EBSD may be expected to provide a more complete representation of high angle boundaries on a given metallographic section, the use of Ga treatment provides for direct 3D imaging of grain structure. The fatigue crack is clearly seen in Figure 2(a), with a number of sharp, apparently crystallographic deflections: the crystallographic nature of the deflections is consistent with the frequent correlation between turning points and grain boundaries (Figs. 2(b) and 3(b)).

It has been widely noted within the literature that the presence of slip band cracking in metallic materials may enhance crack growth resistance via the incidence of RICC at the resultant fracture surface asperities [3–5,14–16], with the present authors, for example, indirectly identifying the influence of dispersoid levels on crack growth resistance in 2024-type materials with varying degrees of fracture surface faceting [14]. Figure 4 highlights a crystallographic assessment of the faceting, with suitable orthogonal sections being made to relate the local crack plane to the associated EBSD determination of the local grain orientation (Fig. 4(b)).

Analysis across the crack width indicated that much of the fracture surface shown was within $\pm 5^\circ$ of $\{001\}$ or $\{111\}$ orientations, with the more steeply inclined sections (as in Fig. 4) exhibiting near- $\{111\}$ orienta-

tions, consistent with a shear dominated slip band propagation mode.

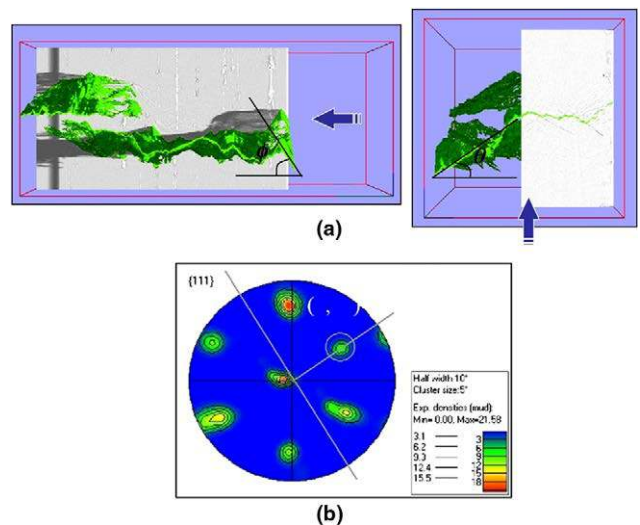


Figure 4. 3D representations of the crack region associated with the sections in Figure 2, highlighting (a) local crack orientation measurement, and (b) associated $\{111\}$ pole figure and crack plane normal.

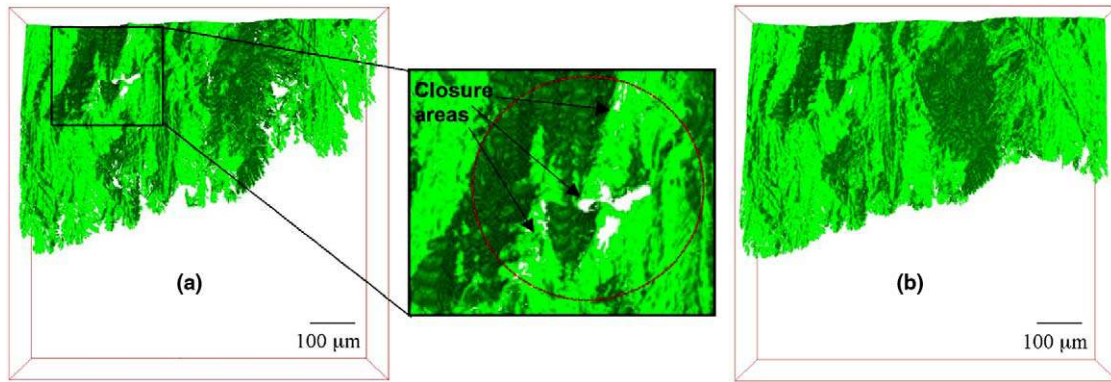


Figure 5. Crack volume, viewed along loading direction at: (a) minimum load, and (b) maximum load. Region of crack closure associated with the {111} oriented ridge in Figure 4 is highlighted in (a).

Figure 5 highlights the associated local incidence of crack closure. Specifically, the crack volume is imaged on its own, and viewed along the direction of loading, i.e. the growth direction lies in the plane of the image, with the crack tip along the lower edge of the areas shown. The same region is shown at the minimum and maximum loads of the fatigue cycle in Figure 5(a) and (b), respectively; as such, regions of crack closure in the wake are identified with the white patches (i.e. no crack volume) in Figure 5(b) which become filled in Figure 5(a). In particular a large patch of closure is identified with the large ridge of {111} crack growth highlighted in Figure 4. This is seen towards the ‘front’ end of the ridge (closer to the crack tip), consistent with previous RICC modelling [15,16].

4. Conclusions

A synthesis of 2D and 3D characterisation tools has been shown to provide a uniquely direct insight into crack closure processes associated with crystallographically rough crack paths, with the incidence of closure at sharp, slip band features confirming prior indirect observations.

Acknowledgements

The authors are pleased to acknowledge the financial and technical support of Alcan Centre de Recherches de Voreppe (CRV), and the assistance of Elodie Boller in the use of the beamline at ESRF.

References

- [1] W. Elber, *Damage tolerance in aircraft structures: ASTM STP486*, ASTM, Philadelphia (PA), 1971, p. 230.
- [2] N. Walker, C.J. Beevers, *Fatigue Eng. Mater. Struct.* 1 (1979) 135.
- [3] S. Suresh, G.F. Zamiski, R.O. Ritchie, *Metall. Trans. A* 12 (1981) 1435.
- [4] S. Suresh, *Fatigue of materials*, Cambridge University Press, Cambridge, 1998.
- [5] K.T. Venkateswara, R.O. Ritchie, *Int. Metall. Rev.* 37 (1992) 153.
- [6] J.K. Shang, R.O. Ritchie, *Acta Metall.* 37 (1989) 2267.
- [7] H. Toda, I. Sinclair, J.-Y. Buffière, E. Maire, K.H. Khor, P. Gregson, et al., *Acta Mater.* 52 (2004) 1305.
- [8] H. Toda, I. Sinclair, J.-Y. Buffière, E. Maire, T. Connolley, M. Joyce, et al., *Philos. Mag. A* 83 (2003) 2429.
- [9] A. Guvenilir, T.M. Breunig, J.H. Kinney, S.R. Stock, *Acta Metall.* 45 (1997) 1977.
- [10] A. Guvenilir, T.M. Breunig, J.H. Kinney, S.R. Stock, *Trans. Roy. Soc. Lond. A357* (1999) 2755.
- [11] British Standard/International Standard BS ISO12108: 2002. British Standards Institute, London.
- [12] W. Ludwig, *Development and applications of synchrotron radiation microtomography*, PhD Thesis, University of Munich, 2001.
- [13] K.H. Khor, J.-Y. Buffière, W. Ludwig, H. Toda, H.S. Ubhi, P.J. Gregson, et al., *J. Phys: Condens. Matter* 16 (2004) S3511–S3515.
- [14] Y. Xu, P.J. Gregson, I. Sinclair, *Mater. Sci. Forum* 331–337 (2000) 1525.
- [15] M.R. Parry, S. Syngellakis, I. Sinclair, *Mater. Sci. Eng. A* 291 (2000) 224.
- [16] N. Kamp, K.D. Singh, M.R. Parry, I. Sinclair, *Acta Mater.* 52 (2004) 343.